AQUA
Water Infrastructure, Ecosystems and Society



IWA PUBLISHING

 AQUA — Water Infrastructure, Ecosystems and Society Vol 73 No 3, 553 doi: 10.2166/aqua.2024.304

# On the hydraulic performance of the inclined drops: the effect of downstream macro-roughness elements

Farhoud Kalateh [a,*], Ehsan Aminvash [a] and Rasoul Daneshfaraz [b]

[a] Faculty of Civil Engineering, University of Tabriz, Tabriz, Iran
[b] Faculty of Engineering, University of Maragheh, Maragheh, Iran
*Corresponding author. E-mail: f.kalateh@gmail.com; fkalateh@tabrizu.ac.ir

FK, 0000-0001-5192-9408; EA, 0000-0001-8901-2232; RD, 0000-0003-1012-8342

## ABSTRACT

The main goal of the present study is to investigate the effects of macro-roughnesses downstream of the inclined drop through numerical models. Due to the vital importance of geometrical properties of the macro-roughnesses in the hydraulic performance and efficient energy dissipation downstream of inclined drops, two different geometries of macro-roughnesses, i.e., semi-circular and triangular geometries, have been investigated using the Flow-3D model. Numerical simulation showed that with the flow rate increase and relative critical depth, the flow energy consumption has decreased. Also, relative energy dissipation increases with the increase in height and slope angle, so that this amount of increase in energy loss compared to the smooth bed in semi-circular and triangular elements is 86.39 and 76.80%, respectively, in the inclined drop with a height of 15 cm, and 86.99 and 65.78% in the drop with a height of 20 cm. The Froude number downstream on the uneven bed has been dramatically reduced, so this amount of reduction has been approximately 47 and 54% compared to the control condition. The relative depth of the downstream has also increased due to the turbulence of the flow on the uneven bed with the increase in the flow rate.

**Key words:** flow energy dissipation, Froude number, inclined drop, numerical simulation

## HIGHLIGHTS

- The use of macro-roughness elements downstream of the inclined drop for the first time.
- Using two geometries for macro-roughness elements.
- Examining the influence of the inclined drop angle and also the different states of the macro-roughness elements.

## GRAPHICAL ABSTRACT

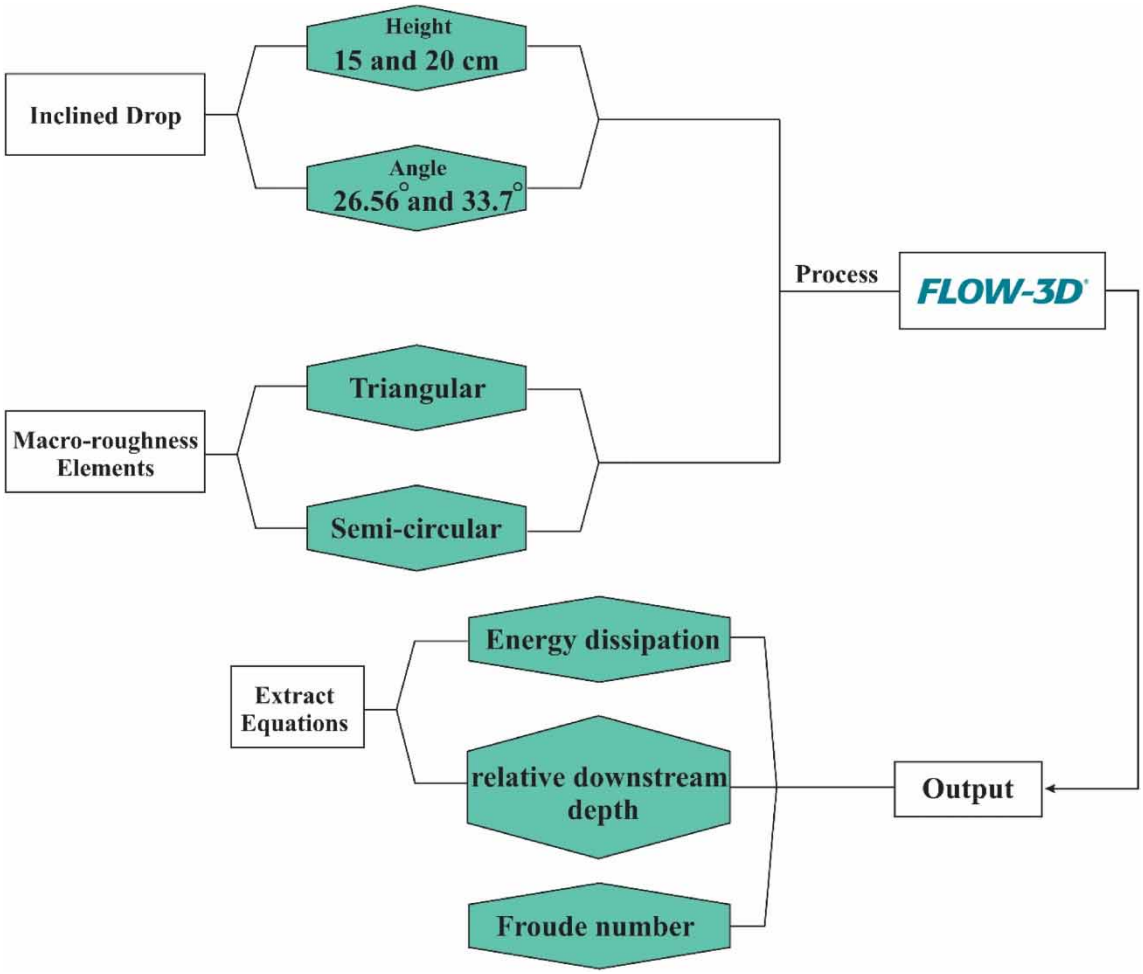


## 1. INTRODUCTION

In water treatment systems, infrastructure design, water transmission lines, eroding waterways, and water transmission network systems, and also when the natural slope of the land is high, the percentage of using structures called inclined drops increases. Inclined drops are structures that cause increased destructive energy loss, decreased speed, and increased pressure. Due to the high flow energy downstream of the drops, over time, the downstream structures are damaged, destroyed, and scoured, causing a lot of damage. Therefore, to reduce destructive energy downstream, depreciating structures should be used. Creating turbulence and forming two-phase flows is one of the methods to increase energy consumption. macro-roughness is one of the elements that can be effective in this matter. These elements can be continuously and non-continuously used with various arrangements and cause an increase in energy loss. This research aims is to make an effective proposal with macro-roughness downstream of the rectangular inclined drop on the flow hydraulic parameters. The first studies done in connection with inclined drops related to energy dissipation downstream of these structures were by Wagner (1956); the purpose of this research is to investigate the energy loss drops on the Columbia River. Ohtsu & Yasuda (1991) investigated the hydraulic jumps on the chute with angles of 8°–60°. Hydraulic jump downstream of spillways by Samadi-Boroujeni *et al.* (2013) and AlTalib *et al.* (2015), the hydraulic jump at the place of sudden changes in the channel cross-section by Matin *et al.* (2018), and the hydraulic jump after the flow passes through the sluice gate were studied by Mouaze *et al.* (2005), and Lopardo (2013). Ead & Rajaratnam (2002) stated that the amount of shear stress in a smooth bed is one-tenth of the shear stress on an uneven bed. Canovaro & Solari (2007) conducted dissipative analogies between a schematic macro-roughness arrangement and step–pool morphology. Results showed that the comparison between the present results and flow

resistance evaluated for step–pools reproduced in the laboratory and observed in the field suggests that step–pool streams are characterized by a bed geometry able to develop the maximum flow resistance. Pagliara *et al.* (2008) studied the energy loss on rough ramps. Ghare *et al.* (2010) designed a roughened chute with several inclines to investigate the relative energy consumption, and the research results show that the trend of flow energy dissipation decreases with the increase of the relative critical depth in all the designed slopes. Katourani & Kashefipour (2012) investigated the effect of the space and the size of the blocks installed on the inclined slope experimentally. The results of their research show an increase in energy dissipation with an increase in the width of the blocks and the porosity space between them. The study of the effect of the geometry of the stilling basin on the energy consumption of the roughened inclined drop has been investigated by Pagliara & Palermo (2012). Also, Pagliara *et al.* (2015) investigated the energy dissipation over large-scale roughness for both transition and uniform flow conditions. The findings of their research showed that the energy dissipation rate slightly increases with the boulder concentrations for the tested slopes and materials.

The results showed that with the increase of the relative critical depth, the energy loss had a downward and decreasing trend. The loss of energy on a roughened drop using coarse and fine sand has been investigated by Abbaspour *et al.* (2019, 2021), and the results showed that the energy dissipation of flow in a rough inclined drop is at most 32% higher than that of a smooth drop. Daneshfaraz *et al.* (2021a) investigated the effect of the geometry of roughness elements on the hydraulic parameters of the inclined drop. In their research, they used roughness elements with bat-shaped, cylindrical, and triangular geometries, and the results showed that the amount of flow energy dissipation in bat-shaped, cylindrical, and triangular elements was 85, 76, and 65% higher, respectively, than that of a smooth drop without roughness. Also, Daneshfaraz *et al.* (2021b) used the support vector machine algorithm to predict the hydraulic parameters of flow in a rough bed with a divergent stilling basin. Dey & Sarkar (2008) showed that with the increase in the size of the macro-roughnesses, the velocity distribution takes on an increasing trend. Energy loss due to free hydraulic jump for different roughness geometries has been discussed by Tokyay *et al.* (2011). Meanwhile, Akib *et al*. (2015) and Roushangar & Ghasempour (2019) focused their research on the relative depth, relative length of the hydraulic jump, and the characteristics of two-phase slows of weather and energy dissipation in unsmooth beds. Pourabdollah *et al.* (2018) compared the kind of hydraulic jumps in roughened and uneven beds with reverse slopes. Numerical simulations have been used by various researchers to investigate hydraulic jump characteristics. Federico *et al.* (2019) used the smoothed-particle hydrodynamic (SPH) method, Bayon-Barrachina & Lopez-Jimenez (2015) used the OpenFOAM model, and Witt et al. (2018) used the CFD model to investigate the hydraulic jump, and Shekari *et al.* (2014) used it for submerged hydraulic jump. Parsaie *et al.* (2016) carried out a numerical study of cavitation on flip bucket overflow. Results showed that the main difference between numerical and physical modeling is related to the head of the velocity, which is considered in physical modeling. Fang *et al.* (2018) examined the influence of permeable beds on hydraulically macro-rough flow. Results showed that near the bed, the relative magnitude of turbulent events shows a transition from an ejections-dominating to a sweeps-dominating zone with vertical distance.

Farahi Moghadam *et al.* (2019) examined a numerical approach to solve fluid–solid two-phase flows using the time-splitting projection method with a pressure-correction technique. The results show the high capability in dynamic simulation of water and sediment flows either at the flow depth or along the channel. Also, in another study, Farahi Moghadam *et al.* (2020) conducted the time-splitting pressure-correction projection method for complete two-fluid modeling of a local scour hole. Results showed that the capacity of the model for simulating the longitudinal fluid velocity and sediment concentration in a local scour hole was evaluated.

Hajiahmadi *et al.* (2021) conducted the experimental evaluation of vertical shaft efficiency in vortex flow energy dissipation. The results showed that the flow energy dissipation rate varied from 26.71 to 51.85%. The experimental data demonstrated that increasing the inflow Froude number and the inlet bottom slope will result in the reduction of the energy dissipation rate in the vertical shaft. Mahmoudi-Rad & Najafzadeh (2023) have shown with the experimental evaluation of energy dissipation on vortex flow in drop shafts that the efficiency of energy loss in vertical shafts varied from 10.8 to 62.29%. Nicosa *et al.* (2023), by investigating the effect of boulders arrangement on the flow resistance caused by the macro roughness of the bed, showed that the Darcy-Weisbach friction factor can be accurately estimated by the proposed flow resistance equation, and the effect of the boulder arrangement on flow resistance law is more evident for low element concentrations. Kurdistani *et al.* (2024) examined the apron and macro-roughness as scour countermeasures downstream of block ramps. Results show that macro-roughness on the ramp and downstream aprons work well as scour countermeasures.

The review of previous studies and research shows that although many studies have been conducted on uneven beds, no research has been done concerning uneven beds with macro-roughnesses downstream of inclined drop. However, more research needs to be done on the effects of different geometries of uneven bed elements in inclined drop structures. The present research aims to use numerical methods based on computational fluid dynamics (CFD) to investigate the hydraulic parameters of the flow, such as the depth of the flow conjugate, relative energy loss, changes in the downstream regime of the structure, etc., in the case of using triangular and semi-circular macro-roughnesses.

## 2. MATERIALS AND METHODS

### 2.1. Introduction of the research model

In the present research, two roughness geometries with semi-circular and triangular shapes have been used continuously to numerically simulate the effect of macro-roughness downstream of the inclined drop. The height and center-to-center distance of the macro-roughnesses are equal to 2 and 6 cm, respectively. The height of the drop structure is equal to 15 and 20 cm, and the angle of the inclined surface of the drop is equal to 26.56° and 33.7°. To verify the numerical data, an experimental model of an inclined drop with a smooth bed downstream in a channel with dimensions of length, width, and height of 5 m, 30 cm, and 45 cm, respectively, and a drop with a height of 15 and 20 cm and an angle of 26.56°, has been used. Figure 1 shows a view of the present research model with the dimensions and macro-roughness used.

### 2.2. Dimensional analysis

According to Figure 1, the effective parameters of the inclined drop with the macro-roughnesses located downstream are in the following equation.

$$f_1(\mu, \rho, g, Q, H, \Pi, E_0, E_1, E_2, y_0, y_c, y_1, y_2, h, l, L_j) = 0 \quad (1)$$

where $\mu$ is the kinematic viscosity, $\rho$ is the specific mass of the fluid, $g$ is the acceleration of gravity, $Q$ is the inlet flow rate, $H$ is the height of the drop, $\Pi$ is the slope angle of the drop to the horizon, $E_0$, $E_1$, and $E_2$ are the specific energies of the upstream, end and downstream of the drop, respectively, $y_c$ is the critical depth, $y_0$, $y_1$, and $y_2$ are the flow depths upstream, end, and downstream of the inclined drop, respectively, $h$ and $l$ are the height and length of the macro-roughness elements, and $L_j$ is the length of the hydraulic jump.

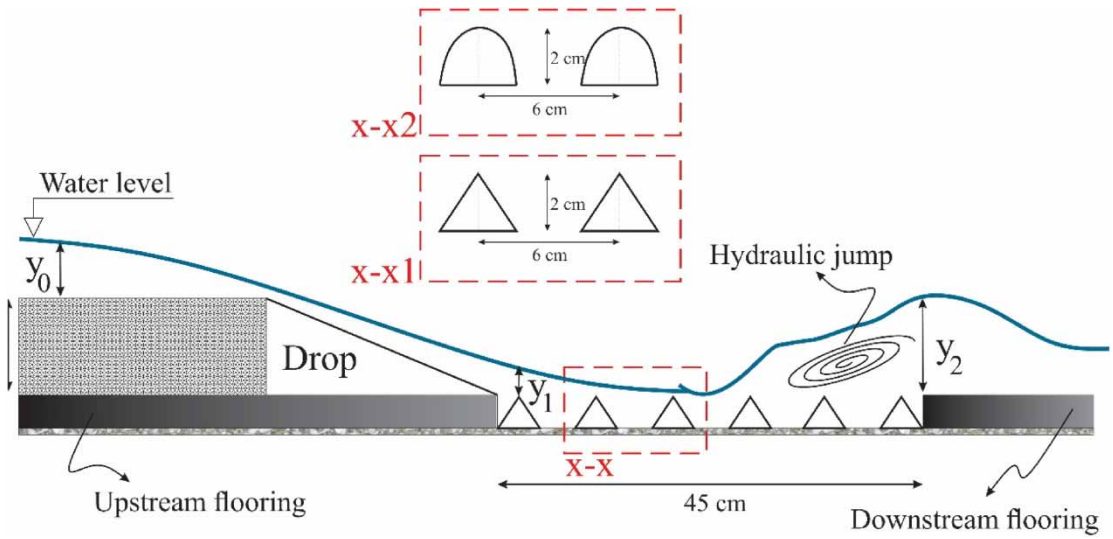


**Figure 1** | Schematic of the present research model with dimensions and macro-roughnesses installed.

The dimensional analysis performed in this research is based on the Buckingham-$\Pi$ theory. The dimensionless parameters were presented in the following equation.

$$f_2\left(\mathrm{Fr}_0, \mathrm{Fr}_2, \mathrm{Re}, \frac{H}{y_c}, \frac{E_0}{y_c}, \frac{E_1}{y_c}, \frac{E_2}{y_c}, \frac{y_0}{y_c}, \frac{y_1}{y_c}, \frac{y_2}{y_c}, \Pi, \frac{h}{y_c}, \frac{l}{y_c}\right) = 0 \tag{2}$$

By simplifying, making it meaningful, and dividing some dimensionless parameters, the independent parameters were presented in Equation (3). Also, since the values of some parameters such as $l$ and $h$ are fixed, they are removed from the parameters. On the other hand, the flow regime is turbulent in all the flow rates of the present research. For this reason, the Reynolds number parameter has been removed.

$$\frac{\Delta E_2}{E_0}, \frac{y_2}{H}, Fr_2 = f_3\left(Fr_0, \theta, \frac{y_c}{H}\right) \tag{3}$$

### 2.3. Evaluation criteria

In this research, four evaluation parameters of root mean square error (RMSE), coefficient of determination ($R^2$) and, Kling–Gupta coefficient (KGE) have been used. It is necessary to explain that better and excellent results are obtained when the RMSE parameter is zero, and the $R^2$ and KGE parameters are 1. The above evaluation criteria presented in Equations (4)–(6), respectively.

$$\mathrm{RMSE} = \sqrt{\frac{1}{N}\sum_{i=1}^{N}(X_{\mathrm{Exp}} - X_{\mathrm{Num}})^2} \tag{4}$$

$$R^2 = \left(\frac{\sum_{i=1}^{N}((X)_{\mathrm{Exp}} - \overline{(X)_{\mathrm{Exp}}}) \times ((X)_{\mathrm{Num}} - \overline{(X)_{\mathrm{Num}}})^2}{\sqrt{\sum_{i=1}^{N}((X)_{\mathrm{Exp}} - \overline{(X)_{\mathrm{Exp}}})^2 \times \sqrt{\sum_{i=1}^{N}((X)_{\mathrm{Num}} - \overline{(X)_{\mathrm{Num}}})^2}}}\right) \tag{5}$$

$$\mathrm{KGE} = 1 - \sqrt{(R-1)^2 + (\beta-1)^2 + (\gamma-1)^2}, \beta = \frac{\overline{\mathrm{Pre}}}{\overline{\mathrm{Obs}}}; \gamma = \frac{\sigma_{\mathrm{Pre}}/\overline{\mathrm{Pre}}}{\sigma_{\mathrm{Obs}}/\overline{\mathrm{Obs}}} \tag{6}$$

To calculate the specific energy of the flow upstream of the inclined drop ($E_0$), the specific energy of the downstream ($E_2$) and also the amount of relative energy dissipation can be calculated through the following equations, respectively.

$$E_0 = H + \frac{3}{2}y_c \tag{7}$$

$$E_2 = y_2 + \frac{v^2}{2g} = y_2 + \frac{Q^2}{2gA^2} = y_2 + \frac{q^2}{2gy^2} \tag{8}$$

$$\frac{\Delta E}{E_0} = \frac{E_0 - E_2}{E_0} \times 100 = 1 - \frac{E_2}{E_0} \times 100 \tag{9}$$

### 2.4. Turbulence model, simulation specifications, and solution field network

The governing equations for the fluid flow in the Flow-3D model are continuity or mass conservation and Navier–Stokes equations. This model solves the mentioned equations with the finite volume method (VOF) on a gridded field to analyze the flow in an incompressible fluid state. The continuity and Navier–Stokes equations are shown in the following equations, respectively.

$$\frac{\partial A}{\partial t} + V\frac{\partial A}{\partial x} + A\frac{\partial V}{\partial x} = 0 \tag{10}$$

$$\frac{\delta U_i}{\delta t_i} + \rho U_i \frac{\partial U_i}{\partial x_i} - \frac{\partial P}{\partial x_i} + \frac{\partial}{\partial x_i}\left(\mu\frac{\partial U_i}{\partial x_j} - \rho u_j' u_i'\right) + \rho g_i \tag{11}$$

where $U_i$ and $u'_i$ are, respectively, the average velocity and the oscillating velocity in the $x_i$ direction, $x_i = (x, y, z)$, $U_i = (U, V, W)$ and $u'_i = (u', v', w')$. $\rho$, $\mu$, $P$, and $g_i$ are specific mass, dynamic viscosity, pressure, and gravitational acceleration, respectively. Instantaneous velocity is obtained using the relation $u_i = U_i + u'_i$ for all three directions. In this research, the RNG, $K$-$\varepsilon$ model, and $K$-$\omega$ model have been used to achieve their goals. According to the validation results of all three investigated turbulence models, the RNG normalized groups method was used to simulate other models of this research. The reason for using the RNG turbulence model is the ability of this model to simulate flow with a high number of meshes, good performance in simulating flow separation areas, and better results against the strain and curvature of flow lines (Daneshfaraz *et al.* 2021a, 2021b). The RNG disturbance model includes two equations which are presented in the following:

$$\frac{\delta U_i}{\delta t_i} + \rho U_i \frac{\partial U_i}{\partial x_i} - \frac{\partial P}{\partial x_i} + \frac{\partial}{\partial x_i}\left(\mu \frac{\partial U_i}{\partial x_j} - \rho u'_j u'_i\right) + \rho g_i ui \tag{12}$$

$$\frac{\partial}{\partial t}(\rho\varepsilon) + \frac{\partial(\rho\varepsilon u_i)}{\partial x_i} = \frac{\partial}{\partial x_j}\left(\alpha_s \mu_{\text{eff}} \frac{\partial k}{\partial x_j}\right) + C_{1s} - \frac{\varepsilon}{k}(G_k + G_{3s}G_b) + C_{2s}.\rho\frac{\varepsilon^2}{k} - R_\varepsilon + S_\varepsilon \tag{13}$$

where $k$ is the turbulent kinetic energy, $E$ is the turbulence dissipation rate, $G_k$ is the production of turbulent kinetic energy due to velocity gradient, and $G_b$ is turbulent kinetic energy production from buoyancy (Daneshfaraz *et al.* 2020, 2021c; Ghaderi *et al.* 2021). In the above equations, $a_k = a_s = 1.39$, $C_{1s} = 1.42$ and $C_{2s} = 1.6$ are model constants. The turbulent viscosity is added to the molecular viscosity to obtain $m_{\text{eff}}$ effective viscosity.

This research, to simulate the effect of macro-roughness elements downstream of a drop with two semi-circular and triangular geometries, from a drop structure with two heights of 15 and 20 cm and with angles of 26.56° and 33.7° to the horizon in a rectangle channel with length and width of 5 m and 30 cm is used according to Figure 1. Table 1 shows the range of variables measured in the present research; in general, 68 simulations were performed in this research.

In the phase of applying the boundary conditions, two mesh blocks have been used due to the sensitivity of the geometric shape of the macro-roughnesses. The first mesh block includes the entire channel and the second mesh block includes the range of macro-roughness elements. Figure 2 shows the solution field with the boundary conditions and also Table 2 shows the characteristics of the boundary conditions in detail.

### 2.5. Verification

To verify the accuracy of the numerical models, an inclined drop experimental model with a height of 20 cm and angles of 26.56° and 33.7° was used. Experiments related to the physical model have been carried out in a flume with dimensions of 0.5 × 0.3 × 5 m (height × width × length) and walls made of clear plexiglass located in a hydraulic laboratory in the University of Maragheh. The depth of the flow was measured by a point gauge with an accuracy of ±1 mm and the flow rate of the flow input was measured by rotameters installed on the pumps with an accuracy of ±2%. An image of the laboratory flume as well as the physical model of the inclined drop is shown in Figure 3.

**Table 1** | The range of variables measured in this research

| $Q$ (L/s) | Height of drop (cm) | $\theta$ (°) | $y_d$ (cm) | $y_c$ (cm) | $Fr_d$ | Shape of macro-roughness elements |
|---|---|---|---|---|---|---|
| 3.33–16.67 | 15 | 26.56 | 2.84–7.87 | 2.32–6.80 | 0.88–3.63 | Semi-circular |
| | | 33.7 | 2.95–8.95 | | 0.82–3.54 | |
| | 20 | 26.56 | 3.25–8.85 | | 0.79–3.57 | |
| | | 33.7 | 3.61–8.97 | | 0.81–3.47 | |
| | 15 | 26.56 | 2.64–7.66 | | 1.21–3.95 | Triangular |
| | | 33.7 | 2.97–8.60 | | 1.12–3.85 | |
| | 20 | 26.56 | 3.15–8.58 | | 0.84–2.15 | |
| | | 33.7 | 3.50–8.95 | | 0.96–1.81 | |
| | 15 | 26.56 | 0.5–2.16 | | 3.98–6.85 | Smooth bed |
| | 20 | | 0.46–1.97 | | 4.67–7.83 | |

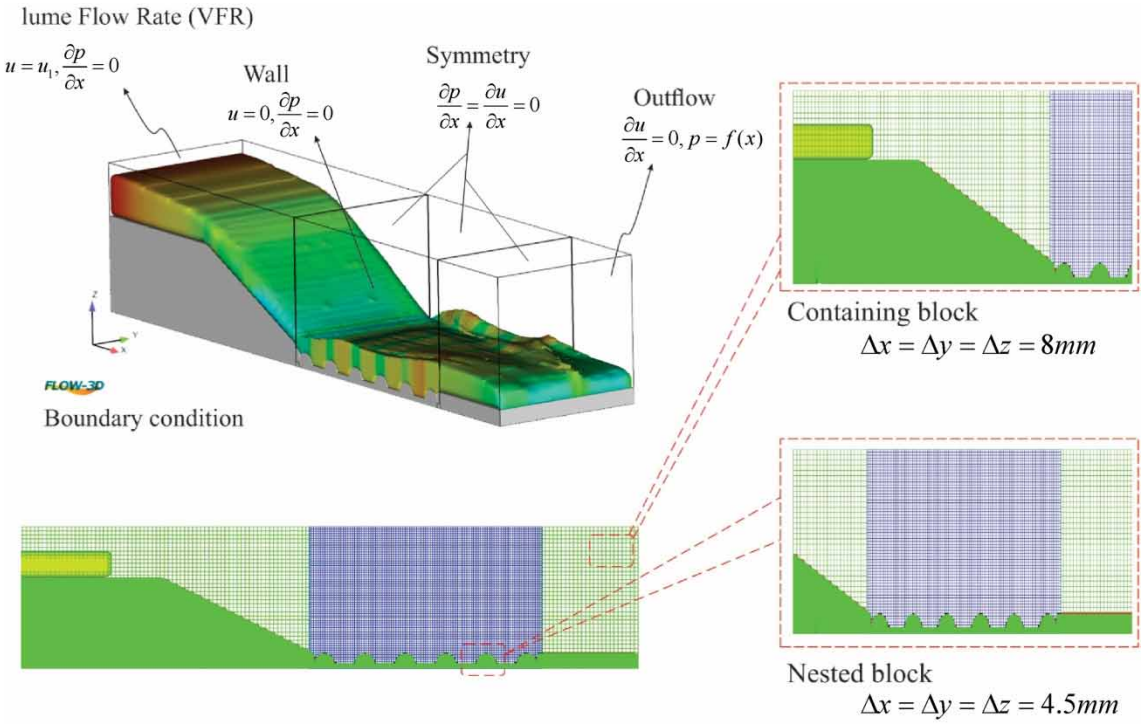


**Figure 2** | Meshing, boundary condition, and solution field network.

**Table 2** | Meshing features and boundary condition

| | *X*-direction | | *Y*-direction | | *Z*-direction | | |
|---|---|---|---|---|---|---|---|
| **Mesh block no.** | **Min** | **Max** | **Min** | **Max** | **Min** | **Max** | **Size of cells (mm)** |
| MB 1 | VFR | Outflow | Wall | Wall | Wall | Symmetry | 8 |
| MB 2 | Symmetry | Symmetry | Wall | Wall | Wall | Symmetry | 4.5 |

In this research, different models have been used to select the optimal network size. Based on what was mentioned in the above materials, RNG, $K$-$\omega$, and $K$-$\varepsilon$ disturbance models were examined for verification, the results of which are summarized in Table 3. According to the results of this table, it can be seen that the RNG model has provided the best results among other selected models.

## 2.6. Sensitivity analysis of mesh

The sensitivity analysis of the cell size was carried out until reaching stable results with little difference between the numerical simulation and experimental results, and the results of the sensitivity analysis are presented in Table 4. Validation has been done based on the parameter of relative energy dissipation ($\Delta E/E_0$), the specifications of the laboratory physical model are described in detail in the above materials and also in Figure 3.

As can be understood from Table 4, test no. 5 with the total number of meshes 864,251 with RMSE, $R^2$, and KGE with 1.13%, 0.978, and 0.974 were selected for simulation. The results of the verification of experimental data with numerical data from Flow-3D are presented in Figure 4. According to Figure 4, it can be seen that the amount of energy dissipation of the numerical model with the height of the inclined drop 20 cm and the angles of 26.56° and 33.7° and with the total number of mesh 864,251 compared to the experimental model has suitable evaluation parameter values and its accuracy with a relative error of $\pm 8.33$ and $\pm 7.85$%, respectively, for angles of 26.56° and 33.7°.

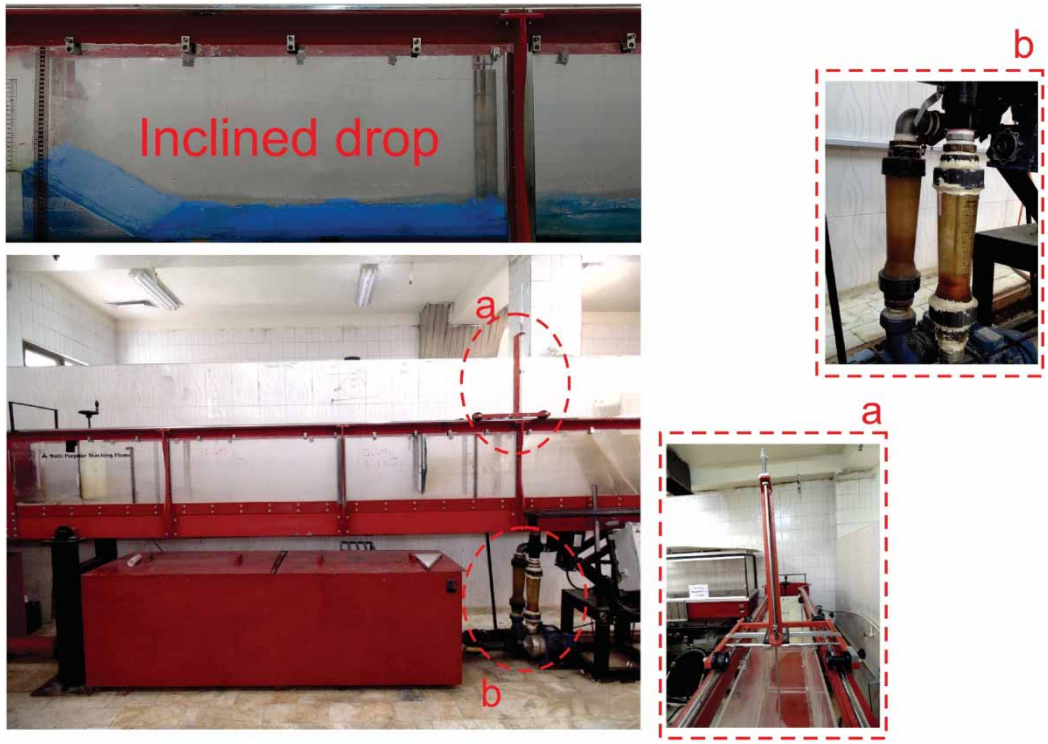


**Figure 3** | Physical and laboratory model of verification of the present research.

**Table 3** | Validation of turbulence models of the present research

| | Criteria evaluation | | | | | | | |
|---|---|---|---|---|---|---|---|---|
| | $H = 20$ cm, $\theta = 26.56°$ | | | | $H = 20$ cm, $\theta = 33.7°$ | | | |
| **Turbulence model** | **RMSE** | **$R^2$** | **KGE** | **DC** | **RMSE** | **$R^2$** | **KGE** | **DC** |
| **RNG** | **0.0163** | **0.957** | **0.963** | **0.951** | **0.0113** | **0.978** | **0.974** | **0.970** |
| *K-ε* | 0.0367 | 0.915 | 0.916 | 0.921 | 0.0341 | 0.905 | 0.908 | 0.911 |
| *K-ω* | 0.0411 | 0.897 | 0.909 | 0.906 | 0.0405 | 0.903 | 0.912 | 0.899 |

Bold values shows that the RNG turbulence model with the presented results was used for simulation.

**Table 4** | Meshing sensitivity analysis and optimal mesh calculation in the RNG model for relative energy dissipation parameter

| **Test no.** | **Turbulence model** | **Total number of meshes** | **RMSE (%)** | **$R^2$** | **KGE** |
|---|---|---|---|---|---|
| Test 1 | RNG | 484,215 | 11.58 | 0.791 | 0.781 |
| Test 2 | | 541,023 | 9.11 | 0.812 | 0.816 |
| Test 3 | | 605,221 | 7.53 | 0.885 | 0.864 |
| Test 4 | | 632,741 | 5.44 | 0.905 | 0.912 |
| **Test 5** | | **864,251** | **1.13** | **0.978** | **0.974** |

Bold values shows that the RNG turbulence model with the presented results was used for simulation.

To investigate the objectives of the present research, the duration of $t = 14$ s was considered in the general mode for simulating all models, as well as the balance and stabilization of the flow with a time step of 0.001 s. Figure 5 shows the $Q$–$t$ hydrograph for the flow rate of 8.33 L/s. Based on this figure, it is inferred that the duration of $t = 14$ s is enough to reach a stable and balanced state for the flow. Of course, it should be noted that according to the figure, the flow in the present research has reached a stable and equilibrium state in $t = 12$ s.

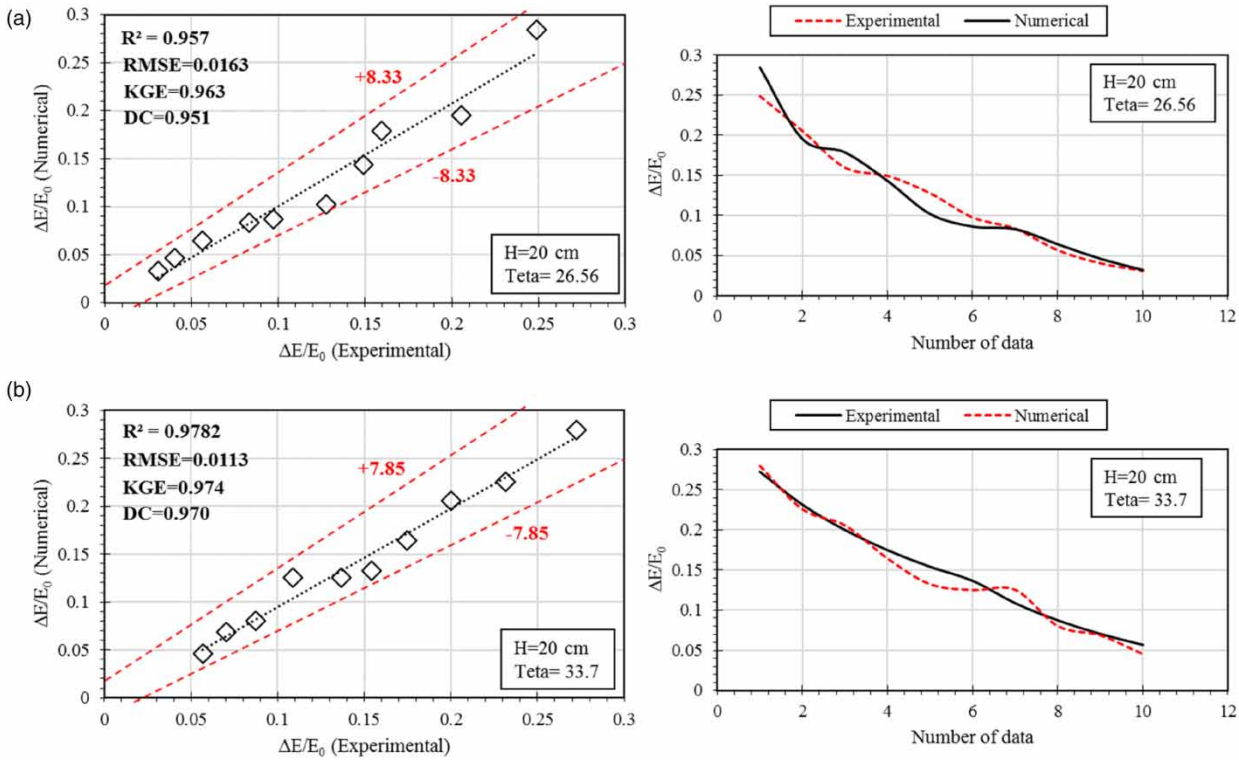


**Figure 4** | Validation of numerical data experimentally based on the parameter of relative energy dissipation for $H = 20$ cm: (a) $\theta = 26.56°$ and (b) $\theta = 33.7°$.

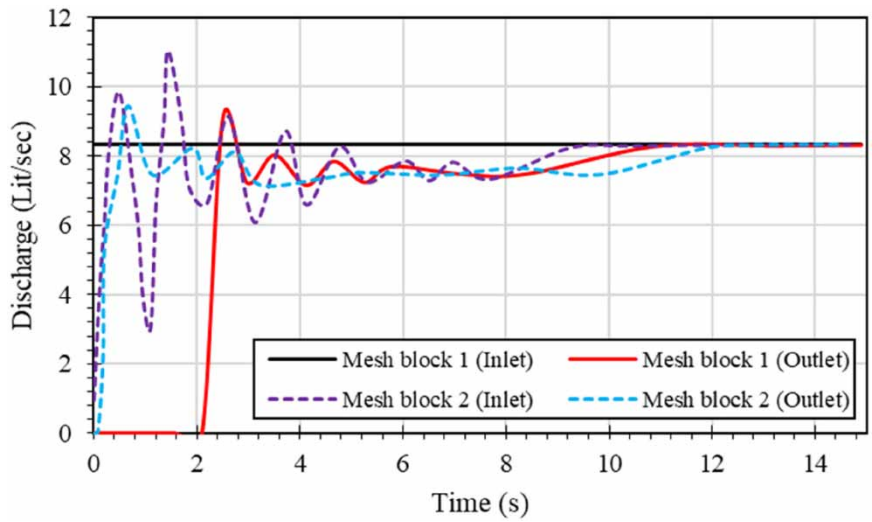


**Figure 5** | *Q–t* hydrograph diagram of equilibrium and flow rate stability.

## 3. RESULTS AND DISCUSSION

### 3.1. Longitudinal profiles of flow

The longitudinal profile of the flow on the uneven bed and at the location of the macro-roughness elements at the flow rates of 10 and 16.67 L/s is presented in Figure 6. It can be seen carefully in these figures that the flow enters the uneven bed after

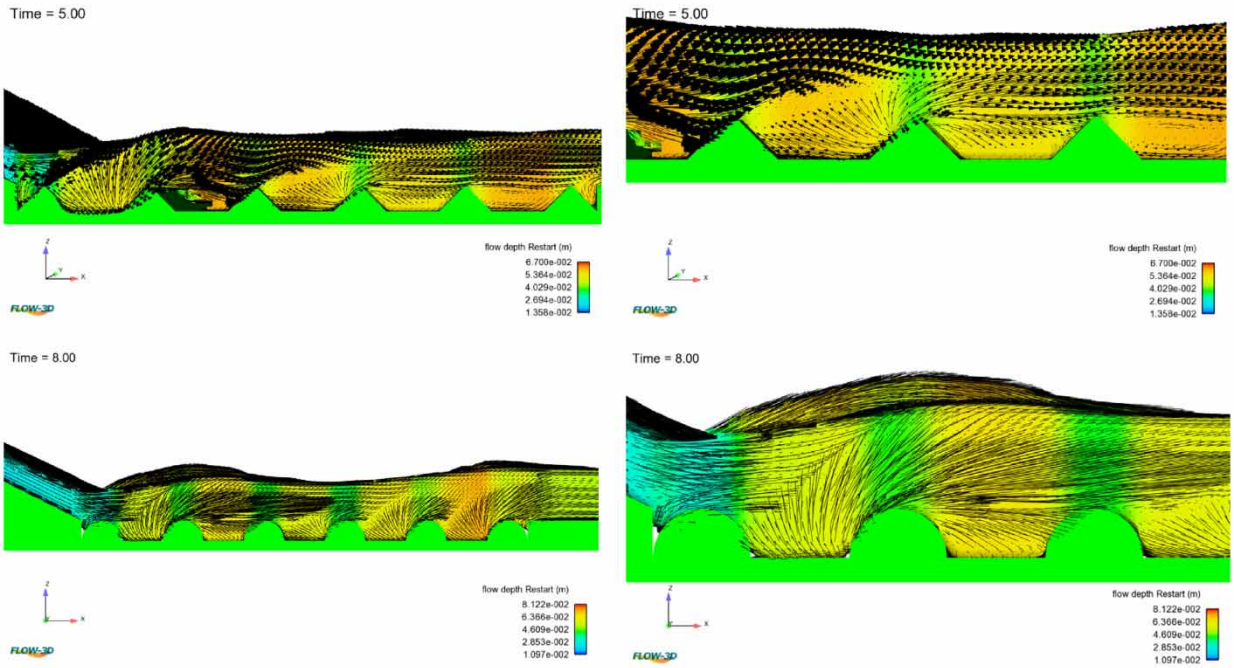


**Figure 6** | Longitudinal profile of flow on macro-roughnesses.

falling from the inclined drop. The uneven bed includes semi-circular and triangular macro-roughnesses parallel to the channel with a height of 2 cm and an axis-to-axis distance of 6 cm in a range of 45 cm. From these figures, it is inferred that in semi-circular and triangular macro-roughnesses, the flow is created after encountering the first element of a flow recoil profile. After that, eddy flows are created in the spaces between the macro-roughness elements, and it is these eddy flows that cause turbulence.

The behavior of semi-circular elements is more than that of triangular elements. So that according to the shapes in the semi-circular elements, swirling flow and turbulence are created between each of the macro-roughness, while in the triangular macro-roughness, the flow after hitting the elements is directed to the downstream section in a projectile manner, and swirling flow is created only in some cases. It is for this reason that more energy loss occurs in semi-circular elements than in triangular elements.

### 3.2. Energy dissipation

Figure 7 shows the energy consumption against the critical depth. Figure 7(a) and 7(b) are related to semi-circular macro-roughnesses, Figure 7(c) and 7(d) are related to triangular macro-roughnesses, and Figure 7(e) is related to the comparison of models with each other. From these figures, it can be seen that with the increase of the relative critical depth and flow rate in all the present research models, the rate of flow energy dissipation is decreasing. Although the relative energy loss has a downward trend, it can be seen that the use of macro-roughnesses has greatly increased the relative energy loss compared to the smooth state of the channel bed. This increase in energy dissipation in semi-circular elements is more than in triangular elements. The reason for this is that in semi-circular elements, the formation of rotating and two-phase flows and the increase of turbulence between the space of macro-roughness and the turbulence of flow lines are greater than in triangular elements. So that this amount of increase in energy loss compared to the smooth bed in semi-circular and triangular elements is 86.39 and 76.80%, respectively, in the inclined drop with a height of 15 cm and 86.99 and 65.78% in the drop with a height of 20 cm. On the other hand, by further examining the models, it was found that the higher the height and angle of the drop incline chute, the more energy loss will follow. The title 'Simple' on the diagram legend of the following figures indicates an inclined drop with a smooth downstream and no macro-roughness elements. Also, the title 'Pi' indicates the slanting angle.

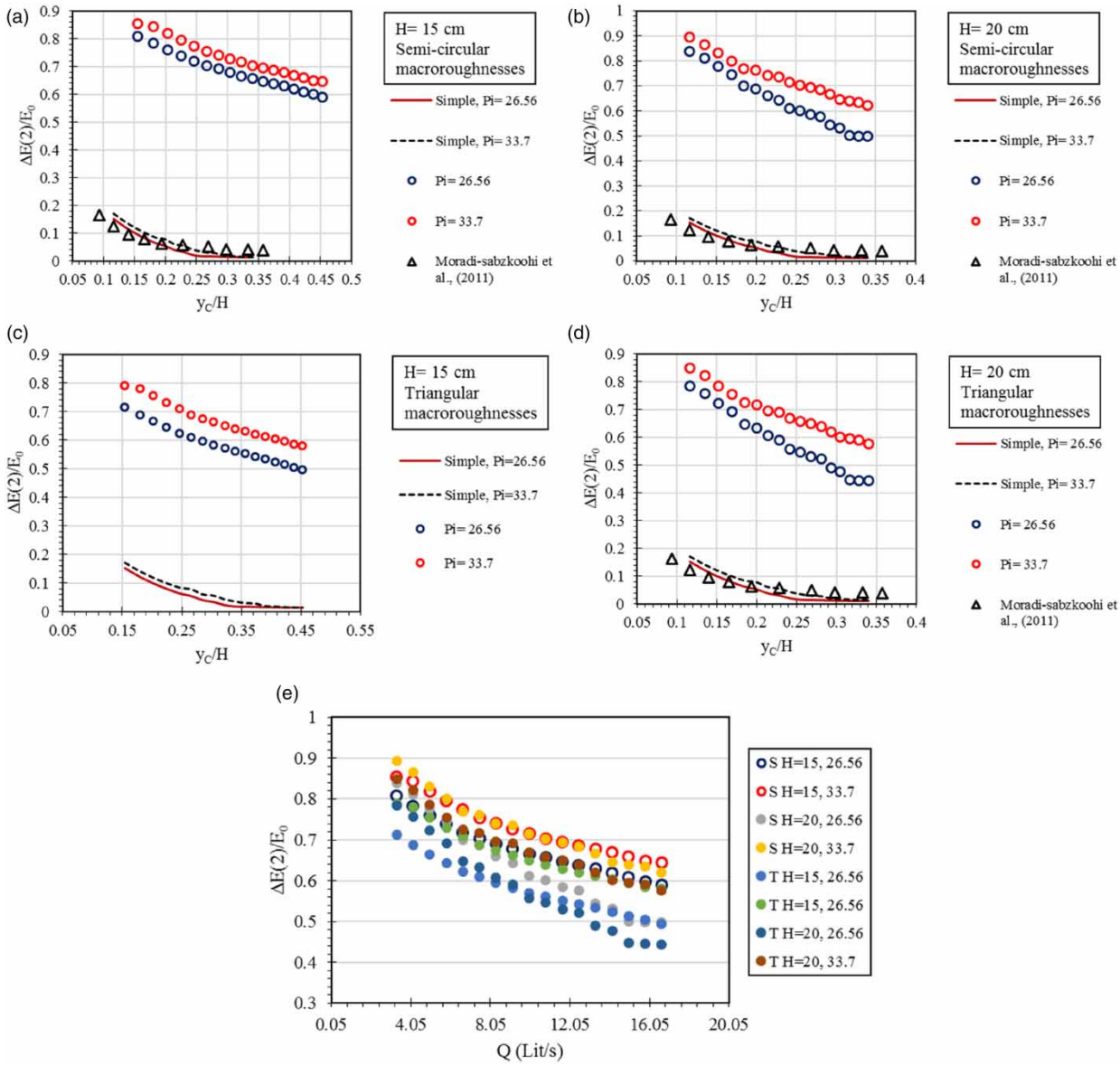


**Figure 7** | Relative energy dissipation vs. the relative critical depth and flow rate: (a,c) $H = 15$ cm, (b,d) $H = 20$ cm, and (e) compare all models with $Q$ (L/s).

On the other hand, the comparison of the present research with the research of Moradi-sabzkoohi *et al.* (2011) shows that in the case of simple inclined drop without using macro-roughness elements, the results are in very good agreement with the numerical data of the present research, but with the use of macro-roughness elements, energy dissipation compared to the research of Moradi-sabzkoohi *et al.* (2011) has increased to a great extent. So that this increase in the inclined drop with a height of 15 cm is 81.5 and 80.17%, respectively, at the angle of 26.56° and 33.7° and by 82.37 and 81.5% in the inclined drop with the height was 20 cm.

### 3.3. Downstream relative depth

Figure 8 shows the amount of downstream relative depth changes of the inclined drop and on the uneven bed against the relative critical depth. Figure 8(a) and 8(b) are related to semi-circular elements, and Figure 8(c) and 8(d) are related to

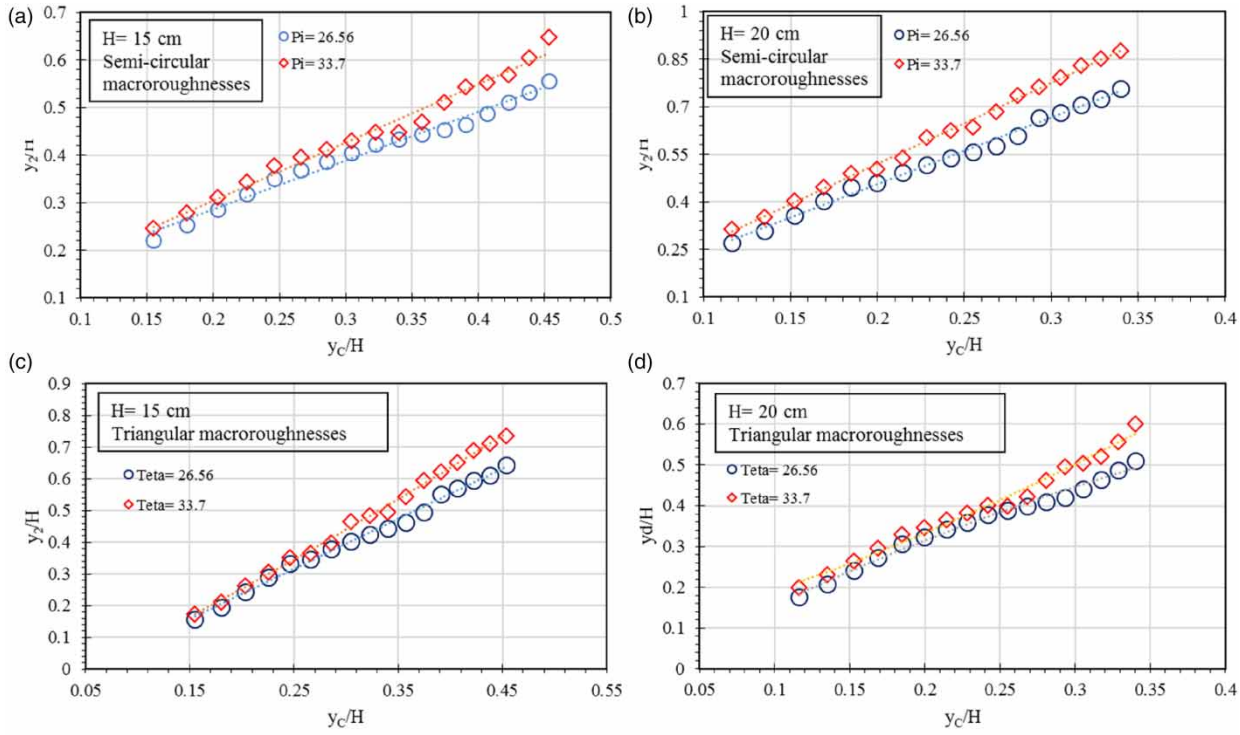


**Figure 8** | Relative downstream depth vs. relative critical depth: (a,c) $H = 15$ cm and (b,d) $H = 20$ cm.

triangular macro-roughness. The figures indicate an increase in the downstream relative depth with an increase in flow rate and relative critical depth in all models of the present research. As the flow rate increases, the flow moves downstream with a higher velocity on the inclined drop. When the flow enters the uneven section and collides with the macro-roughness, the flow turbulence increases and the flow lines are out of order, causing air and weather interference and two-phase flows are formed (Figure 8). Due to the creation of turbulence, the depth of flow downstream of the channel and on the uneven bed has increased, which has finally increased the relative depth downstream. So the effect of semi-circular elements on the downstream depth is relatively greater than triangular elements. On the other hand, the increase in height and also the increase in the sloping surface of the inclined drop have increased the downstream depth. The reason for this is that with the steepening of the slope and the increase in the height of the structure, the velocity of falling of the flow from the structure to the downstream increases.

### 3.4. Downstream Froude number

The Froude number in hydraulic structures is one of the most important parameters that should be investigated. Reducing the amount of the downstream Froude number of hydraulic structures is done by various additional structures, such as stilling basins, rough beds, uneven beds, screens, and so on. Figure 9 shows the graph of the changes in the downstream Froude number against the relative critical depth. It can be seen carefully in the figures that the Froude number has a downward trend in the inclined drop downstream position of the macro-roughnesses with the increase in flow rate and the Froude number has decreased. The results show that compared to the smooth bed without unevenness, the Froude number has decreased significantly. So the range of Froude number in the smooth bed is from 3.98 to 6.85 and from 1.12 to 3.84 in the triangular elements and from 0.88 to 3.63 in the triangular elements with 47 and 53.94% changes compared to the state it has simply changed. It is also necessary to mention that the increase in the height and slope of the inclined chute of the drop causes a further decrease in the downstream Froude number.

The entry of the flow into the uneven bed and dealing with the macro-roughness causes the creation of a hydraulic jump. Hydraulic jump caused changes to the flow regime from supercritical to subcritical. The flow of water after falling from the

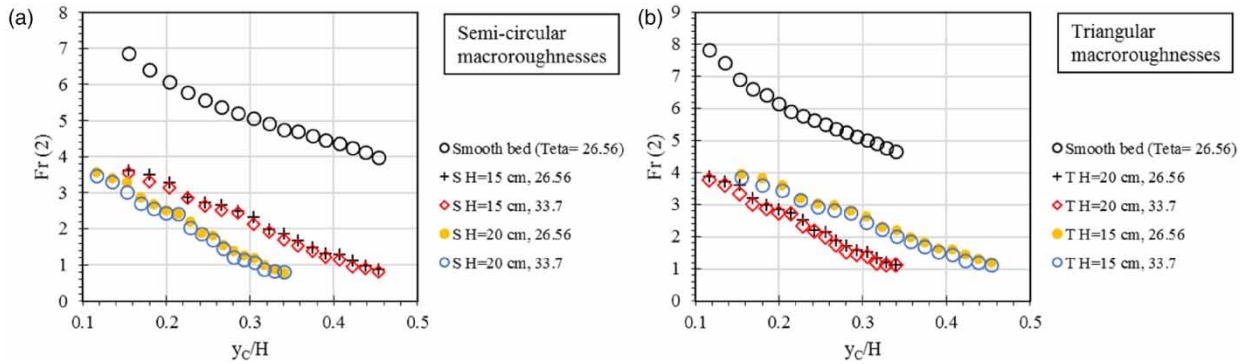


**Figure 9** | Changes in the downstream Froude number: (a) semi-circular; (b) triangular macro-roughnesses.

inclined drop is transferred downstream with high velocity, shallow depth, and supercritical regime. When the flow collides with the macro-roughness elements, the formed hydraulic jump causes a change in the flow regime.

### 3.5. Extraction of nonlinear multivariate equations (SPSS)

To investigate the effect of independent parameters and also to estimate the values of relative downstream depth and relative energy dissipation, equations were presented. The presented equations are obtained with the SPSS model and nonlinear multivariate regression model. Equation (14) is presented to estimate relative energy dissipation and relative downstream depth, and the values of constant parameters and their evaluation criteria are shown in Table 5. It is necessary to explain that in the following equations, the parameter $\theta$ is in terms of radians.

$$\frac{\Delta E_2}{E_0} = a(\mathrm{Fr}_0)^{\mathrm{b}} \times c\left(\frac{y_{\mathrm{c}}}{H}\right)^{\mathrm{d}} \times (\theta)^{\mathrm{e}} \tag{14}$$

$$\frac{y_{\mathrm{d}}}{H} = \frac{a(\frac{y_{\mathrm{c}}}{H})^{\mathrm{b}} \times (\theta)^{\mathrm{c}}}{d(\mathrm{Fr}_0)^{\mathrm{e}}} \tag{15}$$

where $\Delta E_2/E_0$ is the relative energy dissipation, $\mathrm{Fr}_0$ is the upstream Froude number, $y_{\mathrm{c}}/H$ is the relative critical depth, $\theta$ is the slope angle of the drop, and $y_{\mathrm{d}}/H$ is the critical downstream depth.

After extracting the equations to estimate the parameters of relative energy dissipation and the relative depth of the downstream, the values obtained from the numerical data were compared with the output values obtained from Equations (14) and (15), and the results are shown in Figure 10. As it can be inferred from the figure, in both parameters, the numerical data with the output from the equations of the downstream relative depth with the RMSE, $R^2$, and KGE are 0.0377, 0.926, and 0.955, respectively, and with the output obtained from the equation of relative energy dissipation with the values of the above evaluation parameters 0.0437, 0.912, and 0.936 have a very good agreement with each other. Figure 10(c) also shows the comparison of experimental data and the output of the equations provided for the energy dissipation parameter. As it can be inferred from the figure, the experimental data with the output from the equations of the relative energy dissipation with the RMSE and $R^2$ are 0.0346 and 0.9095, respectively.

**Table 5** | Validation of turbulence models of the present research

| | Constant parameters | | | | | Criteria evaluations | | |
|---|---|---|---|---|---|---|---|---|
| **Dependent parameters** | ***a*** | ***b*** | ***C*** | ***d*** | ***e*** | **RMSE** | **$R^2$** | **KGE** |
| $\frac{\Delta E_2}{E_0}$ | 0.8013 | − 2.423 | 0.801 | − 0.0325 | 0.531 | 0.0437 | 0.912 | 0.936 |
| $\frac{y_{\mathrm{d}}}{H}$ | 1.527 | 0.0251 | 0.496 | 0.870 | − 7.767 | 0.0377 | 0.926 | 0.955 |

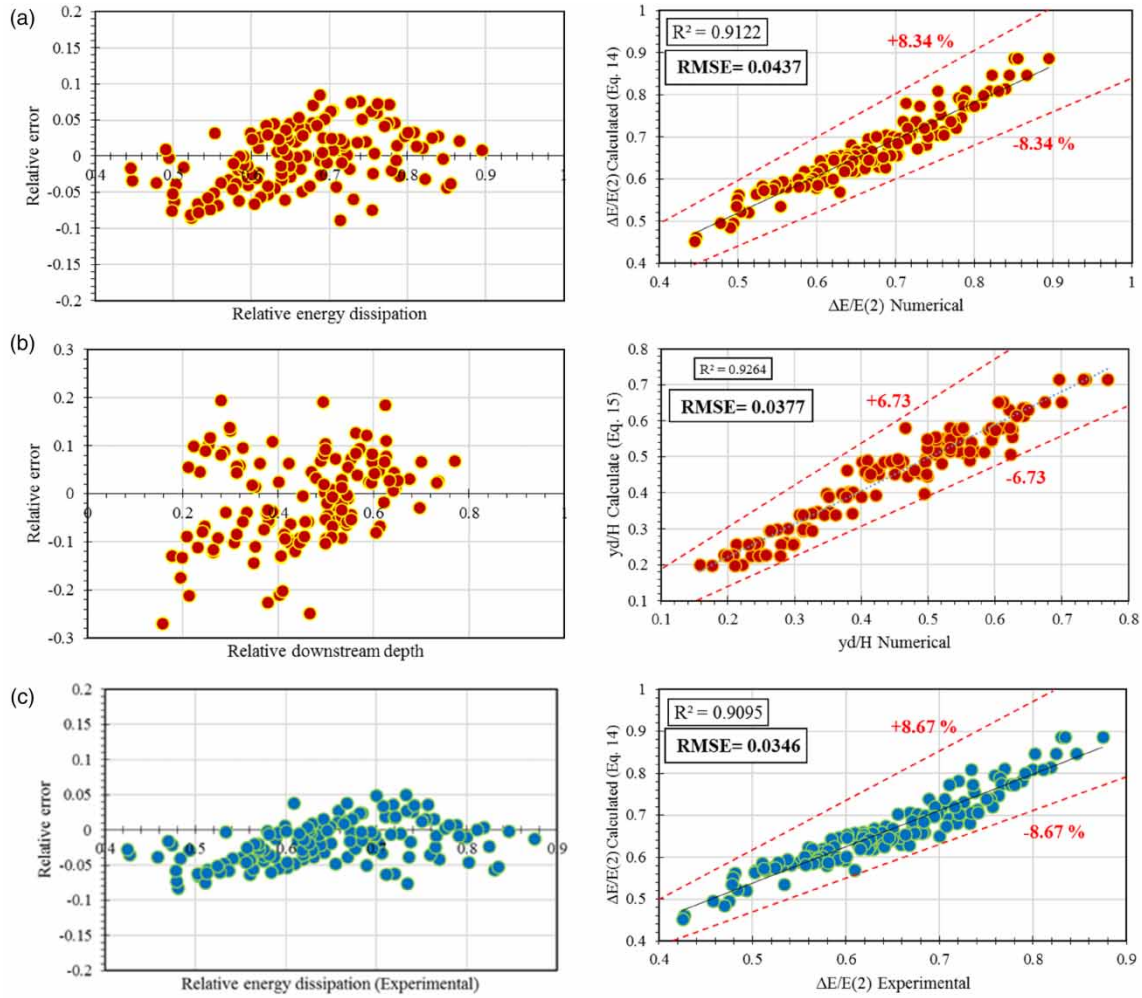


**Figure 10** | Comparison diagram and relative error dispersion of numerical calculation data of energy dissipation and downstream depth: (a,b) Numerical and (c) experimental.

## 4. CONCLUSION

The present research, conducted on the effect of macro-roughnesses with two semi-circular and triangular geometries downstream of the inclined drop, was investigated using the Flow-3D model. In this research, the VOF method and computational fluid dynamics were used to simulate the free surface, and the RNG model was used for the turbulence model. For this purpose, an inclined structure with two heights of 15 and 20 cm and angles of 26.56° and 33.7° was used. Some of the results of the present research can be summarized as follows:

- The present research showed that in general, the amount of relative energy dissipation has taken a downward trend with the increase in the flow rate. This is despite the fact that the energy loss when using macro-roughness has increased compared to the simple state without roughness.
- According to the results of the research, the relative energy loss when using semi-circular and triangular macro-roughness is 86.39 and 76.80% in the drop with a height of 15 cm, and 86.99 and 76.65% in the drop with a height of 20 cm more than the drop with the smooth downstream bed.
- The downstream Froude number of the flow when the fluid flows on the uneven bed has been greatly reduced due to the increase in depth and decrease in the flow velocity compared to the smooth bed, so that these changes are 47 and 53.94% higher than the smooth bed.

- The analysis of the results showed that the relative downstream depth has increased with the increase in discharge due to the high turbulence of the flow, the turbulence of the flow streamlines and the interposition of bubble and water.
- The results of the simulations indicate that when the flow collides with the macro-roughness elements, a hydraulic jump is formed, and for this reason, the relative length of the hydraulic jump has increased with the increase of the relative critical depth.
- Also, by examining the results, it was concluded that the increase in the height and angle of the sloping surface of the inclined drop caused a further increase in the relative energy loss, and the downstream depth, as well as a further decrease in the downstream Froude number.

## FUNDING

No funding was received to assist with the preparation of this manuscript.

## DATA AVAILABILITY STATEMENT

All relevant data are included in the paper or its Supplementary Information.

## CONFLICT OF INTEREST

The authors declare there is no conflict.

## REFERENCES

Abbaspour, A., Taghavianpour, T. & Arvanaghi, H. 2019 Experimental study of the hydraulic jump on the reverse bed with porous screens. *Applied Water Science* **9**, 155.

Abbaspour, A., Shiravani, P. & Hosseinzadeh Dalir, A. 2021 Experimental study of the energy dissipation on rough ramps. *ISH Journal of Hydraulic Engineering* **27**, 334–342.

Akib, S., Ahmed, A. A., Imran, H. M., Mahidin, M. F., Ahmed, H. S. & Rahman, S. 2015 Properties of a hydraulic jump over apparent corrugated beds. *Dam Engineering* **25**, 65–77.

AlTalib, A. N., Mohammed, A. Y. & Hayawi, H. A. 2015 Hydraulic jump and energy dissipation downstream stepped weir. *Flow Measurement and Instrumentation* **69**, 101616.

Bayon-Barrachina, A. & Lopez-Jimenez, P. A. 2015 Numerical analysis of hydraulic jumps using OpenFOAM. *Journal of Hydroinformatics* **17**, 662–678.

Canovaro, F. & Solari, L. 2007 Dissipative analogies between a schematic macro-roughness arrangement and step–pool morphology. *Earth Surface Processes and Landforms: The Journal of the British Geomorphological Research Group* **32**, 1628–1640.

Daneshfaraz, R., Ghaderi, A., Akhtari, A. & Di Francesco, S. 2020 On the effect of block roughness in ogee spill-ways with flip buckets. *Fluids* **5**, 182.

Daneshfaraz, R., Aminvash, E., Di Francesco, S., Najibi, A. & Abraham, J. 2021a Three-dimensional study of the effect of block roughness geometry on inclined drop. *Numerical Methods in Civil Engineering* **6**, 1–9.

Daneshfaraz, R., Aminvash, E., Ghaderi, A., Abraham, J. & Bagherzadeh, M. 2021b SVM performance for predicting the effect of horizontal screen diameters on the hydraulic parameters of a vertical drop. *Applied Science* **11**, 4238.

Daneshfaraz, R., Aminvash, E., Ghaderi, A., Kuriqi, A. & Abraham, J. 2021c Three-dimensional investigation of hydraulic properties of vertical drop in the presence of step and grid dissipators. *Symmetry* **13**, 895.

Dey, S. & Sarkar, A. 2008 Characteristics of turbulent flow in submerged jumps on rough beds. *Journal of Engineering Mechanics* **134**, 49–59.

Ead, S. A. & Rajaratnam, N. 2002 Hydraulic jumps on corrugated beds. *Journal of Hydraulic Engineering* **128**, 656–663.

Fang, H., Han, X., He, G. & Dey, S. 2018 Influence of permeable beds on hydraulically macro-rough flow. *Journal of Fluid Mechanics* **847**, 552–590.

Federico, I., Marrone, S., Colagrossi, A., Aristodemo, F. & Antuono, M. 2019 Simulating 2D open-channel flows through an SPH model. *European Journal of Mechanics-B/Fluids* **34**, 35–46.

Ghaderi, A., Dasineh, M., Aristodemo, F. & Aricò, C. 2021 Numerical simulations of the flow field of a submerged hydraulic jump over triangular macroroughnesses. *Water* **13**, 674.

Ghare, A. D., Ingl, R. N., Porey, P. D. & Gokhale, S. S. 2010 Block ramp design for efficient energy dissipation. *Journal of Energy Dissipation* **136**, 1–5.

Hajiahmadi, A., Ghaeini-Hessaroeyeh, M. & Khanjani, M. J. 2021 Experimental evaluation of vertical shaft efficiency in vortex flow energy dissipation. *International Journal of Civil Engineering* **19**, 1445–1455.

Katourani, S. & Kashefipour, S. M. 2012 Effect of the geometric characteristics of baffle on hydraulic flow condition in baffled apron drop. *Irrigation Sciences and Engineering* **37**, 51–59.

Kurdistani, S. M., Varaki, M. E. & Moayedi Moshkaposhti, M. 2024 Apron and macro roughness as scour countermeasures downstream of block ramps. *ISH Journal of Hydraulic Engineering* 1–9.

Lopardo, R. A. 2013 Extreme velocity fluctuations below free hydraulic jumps. *Journal of Engineering* **2013**, 1–5.

Mahmoudi-Rad, M. & Najafzadeh, M. 2023 Experimental evaluation of the energy dissipation efficiency of the vortex flow section of drop shafts. *Scientific Reports* **13**, 1679.

Matin, M. A., Hasan, M. & Islam, M. R. 2018 Experiment on hydraulic jump in sudden expansion in a sloping rectangular channel. *Journal of Civil Engineering* **36**, 65–77.

Moghadam, K. F., Banihashemi, M. A., Badiei, P. & Shirkavand, A. 2019 A numerical approach to solve fluid-solid two-phase flows using time splitting projection method with a pressure correction technique. *Progress in Computational Fluid Dynamics, an International Journal* **19**, 357–367.

Moghadam, K. F., Banihashemi, M. A., Badiei, P. & Shirkavand, A. 2020 A time-splitting pressure-correction projection method for complete two-fluid modeling of a local scour hole. *International Journal of Sediment Research* **35**, 395–407.

Moradi-SabzKoohi, A., Kashefipour, S. M. & Bina, M. 2011 Experimental comparison of energy dissipation on drop structures. *JWSS - Isfahan University of Technology* **15**, 209–223. (in Persian).

Mouaze, D., Murzyn, F. & Chaplin, J. R. 2005 Free surface length scale estimation in hydraulic jumps. *Journal of Fluids Engineering* **127**, 1191–1193.

Nicosia, A., Carollo, F. G. & Ferro, V. 2023 Effects of boulder arrangement on flow resistance due to macro-scale bed roughness. *Water* **15**, 349.

Ohtsu, I. & Yasuda, Y. 1991 Hydraulic jump in sloping channel. *Journal of Hydraulic Engineering* **117**, 905–921.

Pagliara, S. & Palermo, M. 2012 Effect of stilling basin geometry on the dissipative process in the presence of block ramps. *Journal of Irrigation and Drainage Engineering* **138**, 1027–1031.

Pagliara, S., Das, R. & Palermo, M. 2008 Energy dissipation on submerged block ramps. *Journal of Irrigation and Drainage Engineering* **134**, 527–532.

Pagliara, S., Roshni, T. & Palermo, M. 2015 Energy dissipation over large-scale roughness for both transition and uniform flow conditions. *International Journal of Civil Engineering* **13**, 341–346.

Parsaie, A., Dehdar-Behbahani, S. & Haghiabi, A. H. 2016 Numerical modeling of cavitation on spillway's flip bucket. *Frontiers of Structural and Civil Engineering* **10**, 438–444.

Pourabdollah, N., Heidarpour, M. & Abedi Koupai, J. 2018 Characteristics of free and submerged hydraulic jumps in different stilling basins. In: *Proceedings of the Institution of Civil Engineers-Water Management*. Thomas Telford Ltd, pp. 1–11.

Roushangar, K. & Ghasempour, R. 2019 Evaluation of the impact of channel geometry and rough elements arrangement in hydraulic jump energy dissipation via SVM. *Journal of Hydroinformatics* **21**, 92–103.

Samadi-Boroujeni, H., Ghazali, M., Gorbani, B. & Nafchi, R. F. 2013 Effect of triangular corrugated beds on the hydraulic jump characteristics. *Canadian Journal of Civil Engineering* **40**, 841–847.

Shekari, Y., Javan, M. & Eghbalzadeh, A. 2014 Three-dimensional numerical study of submerged hydraulic jumps. *Arabian Journal for Science and Engineering* **39**, 6969–6981.

Tokyay, N. D., Evcimen, T. U. & Şimsek, Ç. 2011 Forced hydraulic jump on non-protruding rough beds. *Canadian Journal of Civil Engineering* **38**, 1136–1144.

Wagner, W. E. 1956 Hydraulic model studies of the check intake structure-potholes East canal. *Bureau of Reclamation Hydraulic Laboratory Report Hyd*, 411.

Witt, A., Gulliver, J. S. & Shen, L. 2018 Numerical investigation of vorticity and bubble clustering in an air-entraining hydraulic jump. *Computers & Fluids* **172**, 162–180.

First received 21 November 2023; accepted in revised form 29 January 2024. Available online 12 February 2024